Development of fine-tuned top-down mass spectrometry strategies in the chromatographic time scale (LC-TD-MS) for the complete characterization of an anti EGFR single domain antibody-drug conjugate (sdADC)

Rania Benazza[1, 2], Greg Papadakos[3], Jen Thom[3], Helene Diemer[1, 2], Graham Cotton[3], Sarah Cianférani[1, 2] and Oscar Hernandez-Alba[1, 2]

[1] Laboratoire de Spectrométrie de Masse BioOrganique, IPHC UMR 7178, Université de Strasbourg, CNRS, 67087 Strasbourg, France

[2] Infrastructure Nationale de Protéomique ProFI—FR2048, 67087 Strasbourg, France

[3] Almac discovery, Edinburgh Technopole, Milton Bridge, Penicuik, Scotland, EH26 0BE, United Kingdom

Abstract: Even though mAbs have attracted the biggest interest in the development of therapeutic proteins, next generation of therapeutics such as single-domain antibodies (sdAb) are propelling an increasing attention as new alternatives with appealing applications in different clinical areas. These constructs are small therapeutic proteins formed by a variable domain of the heavy chain of an antibody with multiple therapeutic and production benefits compared to their mAb counterparts. These proteins can be subjected to different bioconjugation processes to form single-domain antibody-drug conjugates (sdADC) and hence increase their therapeutic potency, and, akin to other therapeutic proteins, nanobodies and related products require dedicated analytical strategies to fully characterize their primary structure prior to their release to the market.

In this study we report for the first time on the complete sequence characterization of a conjugated anti-EGFR 15 kDa sdADC by using cutting-edge top-down mass spectrometry strategies in combination with liquid chromatography (LC-TD-MS). Mass analysis revealed a highly homogeneous sample with one conjugated molecule. Subsequently, the reduced sdADC was submitted to different fragmentation techniques namely higher-energy collisional dissociation (HCD), electron-transfer dissociation (ETD), and ultraviolet photo-dissociation (UVPD) allowing to unambiguously asses the conjugation site with 16 diagnostic fragment ions and more than 85% of global sequence coverage. The sequence coverage of the non-reduced protein was significantly lower (around 33%), however the thorough analysis of the fragmentation spectra and the inclusion of the internal fragments corroborated the presence of the intra-molecular disulfide bridge along with the localization of the conjugation site.

Altogether, our results pinpoint the complementary of the different fragmentation techniques to provide a thorough analytical characterization of sdAbs-formats even in the chromatographic time-scale, which allows a high-throughput and streamlined analysis of this kind of therapeutic proteins facilitating the implementation on dedicated R&D laboratories.

1. Introduction

Monoclonal antibodies (mAbs) have changed the paradigm of cancer treatment over the last decades with more than 170 approved mAbs world-wide, and more than 200 of mAb biotherapeutics entering clinical studies per year since 2021.[1] However, in oncology, mAbs can encounter tumor resistance mechanisms and their large size comprises penetration into solid tumours, limiting therapeutic efficacy. Thereby, efforts in protein engineering have been focused on the conception of next generation of biotherapeutics to widen their therapeutic applications. Among these entities, single-domain antibodies (sdAb), also known as heavy chain variable domain (VHHs) or nanobodies (originally trademarked in 2003 by Ablynx), have gained increased attention with currently three approved formats on the market[2] and around 37 nanobody candidates undergoing clinical trials[3] so far.

SdAbs derive from the naturally occurring heavy-chain antibodies (HcAbs) in camelids[4]. They are constituted of four relatively constant framework regions along with the three complementarity-determining regions (CDRs) responsible for antigen binding. Thereby, nanobodies are substantially small-sized proteins (~15 kDa) with appealing advantages against their mAb counterparts, *i.e.* better tissue penetration,[6-9] the possibility to bind clefts and cavities of target antigen,[10-11] exhibit lower toxicity and immunogenicity,[12-13] enhanced solubility,[14] and stability,[15] and lower structural heterogeneity. Furthermore, production of sdAbs can be carried out in low-cost systems like *E. coli*[16] or yeast,[17] reducing the overall production cost. For all these reasons, sdAbs have found their way into different applications such as infectious diseases,[18] cancer therapy,[19] and central nervous system (CNS) disorders.[20] Akin to mAbs, nanobodies can be subjected to covalent modifications allowing incorporation of cargo molecules with different properties allowing the use of conjugated nanobodies as drug carriers[21] (single domain antibody-drug conjugate, sdADC) or imaging probes.[22] Similar to other biotherapeutic proteins, the primary structure of sdAbs, and sdADCs has to be thoroughly assessed prior to their commercialization including sequence assessment, identification of post-translational modifications, and the precise localization of the position of the cargo molecules (for conjugated formats) through the development of tailored analytical methods.

The development of complementary activation techniques and their subsequent implementation in last generation high resolution MS platform has paved the way for the development of analytical workflows envisaging protein sequencing at the intact level, *i.e.*, without any prior enzymatic digestion. These strategies are encompassed under the term top-down mass spectrometry (TD-MS) and have been applied to a large variety of biomolecules among which, membrane proteins,[23-26] histones,[27-29] and oligonucleotides.[30-32] MAbs, and derived products such as antibody drug conjugates (ADCs) have also been subjected to TD-MS studies, mainly due to the advent of complementary fragmentation techniques. In most of the cases, a limited proteolysis is performed followed by a reduction step to downsize the mAb-derived protein scaffold,[33-42] and thus mitigating the challenges associated to the fragmentation of 150 kDa proteins with several chains and multiple inter-, and intra-molecule disulfide bridges. However, several examples of TD-MS studies of mAbs,[43-50] and ADCs[51-52] can be found in the literature, illustrating the potential of these methods in the characterization of biotherapeutics at the intact level. More particularly, Loo and coworkers combined ECD and HCD fragmentation (EChcD) to perform TD-MS on one mAb and its conjugated ADC under native conditions,[51] reaching an overall sequence coverage of 70% of both compounds with specific fragment ions allowing the assessment of intra-molecular disulfide bridges and 58% of payload conjugation sites.

Despite the numerous publications showcasing the advantages of TD-MS workflows for intact protein sequencing, sdAbs and sdADCs have been scarcely characterized using these strategies. In 2010, Resemann *et al.* performed the *de novo* sequencing of a 13 kDa nanobody using a TD-MS assisted bottom up (BU) approach.[53] In this case, the fragmentation of the intact nanobody was performed with MALDI in-source decay matrix assisted laser desorption ionization (MALDI-ISD) with two different matrix compositions in order to favor fragmentation of both protein termini, and thus provide an extended protein sequence characterization. A more recent study published by Macias *et al.* applied ultraviolet photo-dissociation (UVPD) activation to fragment three different nanobody-antigen pairs.[54] This experiment was conducted under native MS conditions (nMS) with the main purpose of inferring structural insights onto the quaternary structure of nanobody-antigen pairs from their corresponding UVPD fragmentation spectra. In this context, the fragmentation of the apo-, and holo- forms of the nanobodies were compared to detect significant fragmentation differences upon antigen binding. According to the reported results, the fragment ions originated under both conditions pinpointed a fragmentation suppression located at the antigen-nanobody interfaces leading to the conclusion that UVPD-based native TD-MS can significantly contribute to determine nanobody's paratopes.

As evidenced by the scarce number of reported studies, nanobodies, and their conjugated counterparts have not been extensively studied with TD-MS workflows for their primary structure characterization. Moreover, both studies used direct infusion without providing further evidence demonstrating the suitability of the TD-MS strategies in the characterization of sdAbs in the chromatographic time scale. Here we report for the first time on the characterization of an in-house sdADC using a tailored reversed-phase liquid chromatography top-down mass spectrometry (RPLC-TD-MS) strategy based on higher energy collision induced dissociation (HCD), electron transfer dissociation (ETD), and ultraviolet photo-dissociation (UVPD) techniques. The experimental conditions of each individual activation technique were optimized to improve the fragmentation yield of the peptide backbone, highlighting the advantages/limitations of each fragmentation technique in terms of overall sequence coverage, localization of the conjugation site, and the identification of signature fragment ions to determine the presence of the intra-molecular disulfide bridge. Overall, this study provides a complete picture about the suitability of LC-TD-MS strategies in the characterization of the primary structure of next generation sdAbs, and sdADCs biotherapeutics.

2. Material & methods

2.1 Chemicals and reagents

All buffers and the chemicals used for the protein purification and functionalisation were purchased from Merck. *E. Coli* cells and chitin affinity chromatograpghy resin were purchased from NEB, Luria-Bertani (LB) media, ampicillin (AMP), isopropyl β-D-1-thiogalactopyranoside (IPTG) were purchased form MelfordAlexa Fluor™ 488 C5 Maleimide (AF488) was purchased by ThermoFisher and 5 ml HiTrap desalting columns by Cytiva.

All chemicals were purchased from Sigma-Aldrich (France): acetonitrile (ACN), ammonium acetate ($AcNOH_4$), dithiothreitol (DTT) and trifluoroacetic acid (TFA). RapiGest™ reagent was purchased from Waters (France) and trypsin from Promega (France). All aqueous solutions were prepared with ultra-

pure water system (Sartorius, Göttingen, Germany). LockMass and RDa Calibrant solutions used on the BioAccord were obtained from Waters (Manchester, UK) and the calibration solution used on the Eclipse was a Pierce FlexMix from Thermo Fisher (France). The anti-EGFR nanobody was prepared at Almac Disovery (Scotland, UK).

2.2 Anti-EGFR production, expression, purification and conjugation

sdAb preparation and thiol functionalisation —The anti-EGFR VHH 7C12 cloned to the N-terminus of a GyrA intein-chitin binding domain fusion, was expressed in *E. coli* cells and captured on chitin beads as previously described (cite: https://pubs.acs.org/doi/10.1021/acsmacrolett.8b00461).

The 7C12 intein fusion protein was then cleaved by overnight incubation at room temperature with 200 mM cysteamine in 200 mM NaCl, 50 mM sodium phosphate buffer, pH 6.9, to generate the corresponding C-terminal thiol-functionalised 7C12 protein. Cysteamine excess was further eliminated by size-exclusion chromatography (**Figure S1**).

sdAb conjugation— To conjugate to the C-terminal thiol group of 7C12 (generated by cysteamine cleavage of the precursor intein-fusion protein and referred to as the C-terminal cysteamine thiol), the purified protein was incubated with a 4-fold molar excess of Alexa Fluor 488 maleimide dye at room temperature for 1h. ..The excess dye was removed using a 5 ml HiTrap desalting column equilibrated in PBS, pH 7.4. , The labelling was confirmed by SDS-PAGE and and ESI-TOF MS (Bruker Daltonics) The protein concentration and the degree of labelling were calculated according to the AF488 ThermoFisher manual using the molar extinction coefficient of the protein.

2.3 SEC-nMS analysis

Size exclusion chromatography coupled to mass spectrometry in native conditions (SEC-nMS), was performed using a BioAccord LC-MS system (Waters, Manchester, UK). The assembly comprises an Acquity UPLC M-Class system; including a binary solvent manager, a sample manager at 4°C, a column oven at room temperature, and a UV detector operating at 214 nm and 280 nm, coupled to an RDa detector. Five µg were injected on a BEH SEC 2.1x150 mm 1.7-µm column (Waters) used with an isocratic gradient of 150 mM $AcNOH_4$ (pH 6.9) at a flowrate of 100 mL/min over 6 min. The mass spectrometer was prior calibrated automatically in the positive mode using the calibration solution (Waters) and then operated with a capillary voltage of 3.5 kV and a pressure of 2 mbar. The cone voltage was set to 60V. Acquisitions were performed on the high m/z range 400-7000 with a 1 s scan time.

Data processing was performed using UNIFI v1.913.9 (Waters, Manchester, UK). The avDAR value was calculated using the equation below:

$$avDAR = \frac{\sum_{k=0}^{n} k \times I_k}{\sum_{k=0}^{n} I_k}$$

Where k is the number of drugs and I_k is the relative peak intensity of DAR_k.

2.4 Bottom-up peptide mapping analysis

Sample preparation—ten µg of the sdADC was solubilized in 150 Mm NH_4HCO_3 0.1% RapiGest (Waters) at pH 7.8, to obtain a final volume of 24 µL. Disulfide reduction was performed by incubation of the solution with 5 mM DTT for 30 min at 57°C. 10 mM of IAM for 40 min in the dark at room temperature, was added to alkylate free thiol groups on cysteine residues and prevent reformation of disulfide bridges.

Digestion was performed by adding 5 µL of trypsin solution; *i.e.* 20 µg of trypsin (Promega) suspended in 100 µl of H_2O which corresponds to 1:50 enzyme:substrate ratio, at 37°C for 5h. The reaction was stopped by adding 1% of TFA. RapiGest was eliminated by incubation during 30 min at 37°C and centrifugation at 13,000 g for 10 min.

LC-MS/MS analysis—nanoLC-MS/MS analysis was performed using a Dionex Ultimate 3000 LC system. 100 ng of sdADC digest was trapped on a Symmetry C18 pre-column (180 µm x 20 mm, 5 µm particle size, Waters) and the peptides were separated on an ACQUITY UPLC® BEH130 C18 separation column (75 µm x 250 mm, 1.7 µm particle size, Waters). The solvent system consisted of 0.1% formic acid in water (solvent A) and 0.1% formic acid in acetonitrile (solvent B). Peptide trapping was performed during 3 min at a flow rate of 300 nL/min with 97.5% A and 2.5% B and elution was performed at 40 °C at a flow rate of 300 nL/min from 7.5% to 50% of B in 37 minutes. For optimal nanoLC-MS/MS, the mass spectrometer was operated in positive mode, with the following settings: spray voltage 2000 V and capillary temperature 275°C. The MS scan had a resolution of 120 000, the AGC target was 10^6 and the maximum IT was 50 ms on m/z [300-1800] range. The MS/MS scans had a resolution of 15 000, the AGC target was 10^5 and the maximum IT was 22 ms with an Isolation window of 2 m/z. Top 10 HCD was selected with intensity threshold of 10^4 and dynamic exclusion of 5 s. The normalized collision energy (NCE) was fixed at 30%. The complete system was fully controlled by Thermo Scientific™ Xcalibur™ software. Raw data collected were processed and converted with MSConvert into .mgf peak list format.

Data processing—search engines MASCOT 2.6.2 algorithm (Matrix Science) was used. The search was performed against the sequence of the light and heavy chains of the ADC. Spectra were searched with a mass tolerance of 10 ppm for MS and 0.05 Da for MS/MS data. The search was made without enzyme specified, in order to allow the identification of any non-specific cleavage peptide. Variable modifications were specified: oxidation of methionine residues, pyro-glutamylation of the N-termini, deamidation of asparagine, isomerization of aspartic acid residues and drug-linker conjugation (C52 F H56 N9 O13 and C26 O8 N6 H34) on cysteine residues. Peptide identifications were validated with a minimal Mascot ion score of 20.

2.5 Top-down MS experiments

TD-MS analysis—a Dionex Ultimate 3000 LC system was used to inject one to 3 µg of samples through an Agilent Zorbax 300 SB-C8 (2,1 x 50 mm, 1,8 microns) at 60°C. The solvent system consisted of 0.1% TFA in water (solvent A) and 0.1% TFA in acetonitrile (solvent B). Elution was performed at a flow rate of 200 µL/min from 20% to 60% of B for 7 minutes. All experiments were performed on an Orbitrap Tribrid Eclipse MS (Thermo Scientific). The LC was hyphenated to an Orbitrap Tribrid Eclipse MS (Thermo Scientific) equipped with ETD, HCD and 213 nm UVPD options. For all experiments, the spray voltage was set to 3.4 kV, and the ion transfer tube temperature at 320 °C.

The MS scans were acquired at a resolution of 15 000, the AGC target was 10^6 and the maximum IT at 200 ms on a range of [200-3000] m/z. MS/MS scans had a resolution of 120 000, the AGC target was 10^6 and the maximum IT was 200 ms on m/z [180-2000] with an IW of 2 m/z. The MS scan had a resolution of 120 000, the normalized AGC target was 250% and the maximum IT was 50 ms on m/z [300-1800] range. The MS/MS scans had a resolution of 15 000, the nAGC target was 200% and the maximum IT was 22 ms with an Isolation window of 2 m/z. For HCD fragmentation, the ions were accelerated under a constant N_2 pressure of 10-9 mbar with 12 eV. For performing ETD, anionic fluoranthene radicals were generated in the source region of the instrument. For UVPD, ions were activated with 213 nm laser delivering a total energy of 150 µJ (2 µJ /pulse).

Data analysis— the MS/MS spectra were deconvoluted with Xtract algorithm on FreeStyle software, using a S/N of 3, a fit factor of 70% and a remainder threshold of 25%. The deconvoluted masses were matched to the protein sequence using Prosight Lite algorithm with a 10-ppm ion tolerance to reduce the number of false positives. For each fragmentation method the type of the generated ions was considered, namely b/y in the case of HCD, c/z in the case of ETD, and a/x, b/y and c/z in the case of UVPD. The C-terminus of the protein was modified with a cysteamination, thus the addition of the cysteamine mass was considered on this position. Since the addition of the fluorescent AF488 molecule was targeting the cysteines or the prior added cysteamine, CYS22, CYS96 and the C-terminus was considered to investigate the specific site of conjugation.

To assign the internal fragments, ClipsMS algorithm was used by fixing the parameters as follows: terminal fragments error at 10 ppm and internal fragments error both at 2 ppm, and smallest internal fragment size at 2 AA. The cysteamine and AF488 modifications were considered as localized modifications after confirming their position and type by using ProSight Lite. The fragmentation type and its corresponding generated ions was considered before starting the search.

3. Results

3.1 Intact mass analysis using SEC-nMS

Our in-house sdADC was firstly analyzed using SEC-nMS coupling to determine the experimental mass of the protein, the drug load distribution (DLD), and average drug-to-antibody ratio (avDAR) after conjugation with the surrogate cytotoxic payload molecule AF488 (**Figure 1A,B**Figure 1). The SEC-UV chromatogram reveals a major peak at ~3.88 min corresponding to the monomeric sdADC with an experimental mass of 14 145.7 ± 0.1 Da that can be assigned to the sdAb conjugated to one AF488 molecule (**Figure 1B**). A minor peak is also observed at ~4.50 min corresponding to a fragmented moiety of the AF488 (**Figure S2**). According to this result, the conjugation of the sdAb was complete, leading to an avDAR of 1. This result is in line with the SDS page analysis where the conjugation of the AF488 molecule was confirmed upon UV visualization of the reduced sdADC (**Figure S3**). However, the resolution, and mass accuracy of the SEC-nMS coupling allowed to confirm that the experimental mass of the protein corresponded to the D1 population of the sdADC with a disulfide bridge, suggesting that the integrity of the intra-molecular linkage between both cysteine residues has been maintained during the conjugation process.

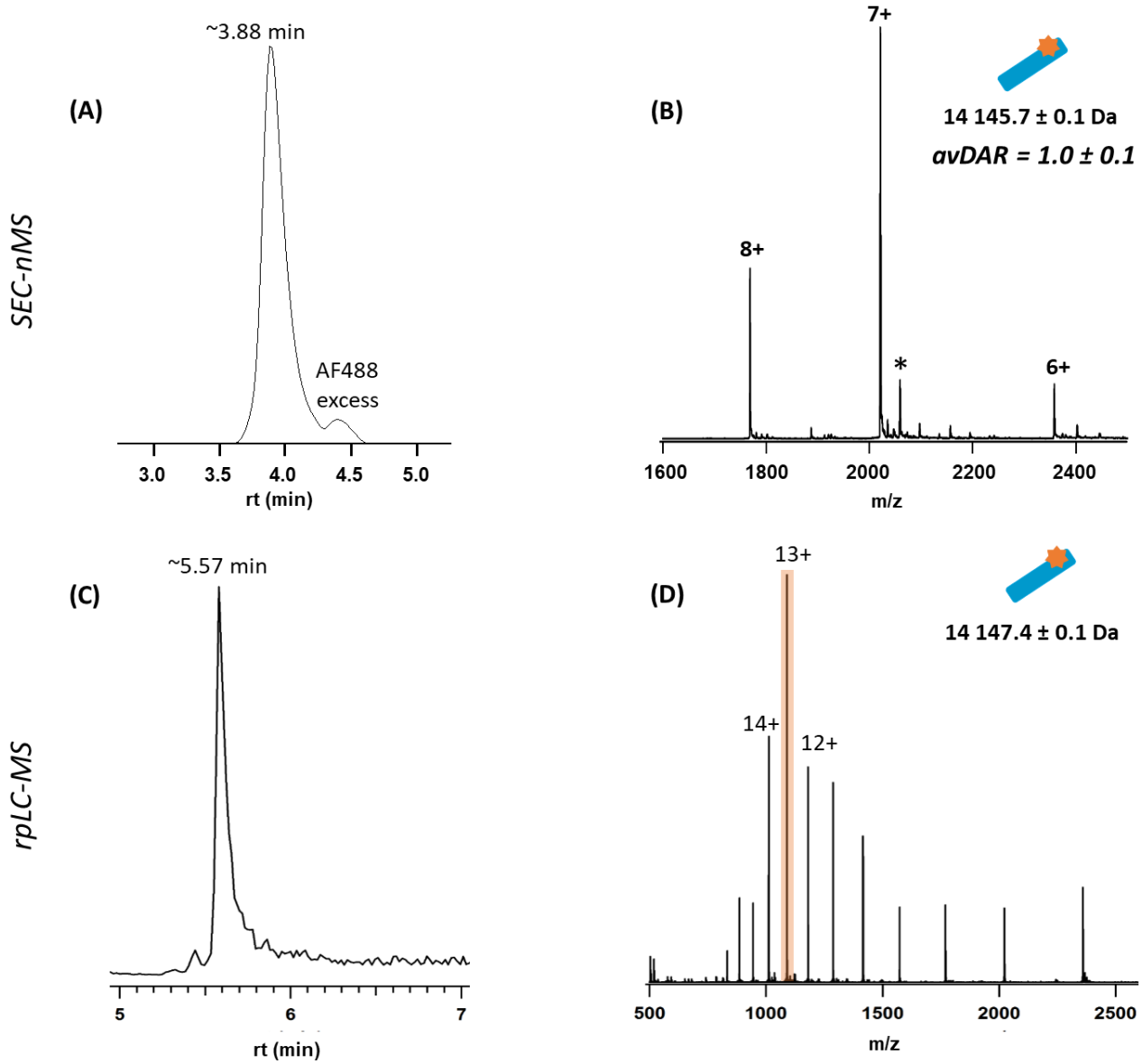

Figure 1: Analysis of unreduced sdADC in native conditions using SEC-nMS (top panel) and in denaturing conditions using rpLC-MS (bottom panel). **(A)** SEC-UV chromatogram. **(B)** MS spectra corresponding to the eluted sdADC in native conditions. **(C)** Total ion chromatogram of the reduced sdADC showing one species at ~5.57 min. **(D)** MS spectra of the reduced sdADC in denaturing conditions.

3.2 Top-down MS for the sequence characterization and conjugation site identification of the sdADC

Recent studies have shown the benefits of TD-MS for the characterization of protein modifications through the direct fragmentation of intact proteins,[27-28, 55-59] although the fragmentation yield is significantly reduced when dealing with large molecular ions (> 30 kDa).[34, 42, 60-62] Taking into account the relative small size of the sdADC, it seems to be the suitable candidate to be subjected to TD-MS workflows in order to perform sequence assessment, along with the localization of the AF488 molecule

in the protein backbone. Since the fragmentation yield of the different activation methods diminishes with the presence of intra-molecular disulfide bonds,[63-65] the conjugation site and the sequence confirmation of the sdADC were carried out upon reduction of the cysteine residues (see material and method section, **Figure 1C, D**). The reduction of the disulfide bridge along with the use of chaotropic agents disrupt the secondary and tertiary structures of the protein, allowing the accommodation of higher number of protons during the ESI process, and thus increasing the overall net charge state of the molecular ions. One major peak centered at ~5.57 min is observed in the chromatogram profile of the sdADC. The charge envelop was centered at the 13+ charge state, and the corresponding experimental mass associated to the main peak was 14 147.6 ± 0.2 Da, in line with the reduced form of the sdADC bearing one AF488 molecule (+ 757.12 Da) **(Figure 1D)**.

Subsequently, the reduced sdADC was analyzed using rpLC-TD-MS using different activation techniques such as HCD, ETD, and UVPD. Optimization of the fragmentation reaction and the charge state of the precursor molecular ions were conducted on the unconjugated sdAb as a reference sample (**Figure 1C-D**). Three charge states (12+, 13+ and 14+) were selected for HCD fragmentation combined with collision energies from 10 to 30 NCE. Interestingly, fragmentation of the 13+ precursor ion gave rise to the largest number of fragments leading to a sequence coverage of 28% (*versus* 20% and 27% for 12+ and 14+, respectively, **Figure S4A**). Moreover, the activation energy was also optimized, reaching 31% of sequence coverage with 20 NCE (**Figure S4B**).

The optimized fragmentation conditions were applied to the sdADC. Overall, similar fragmentation spectra of sdAb, and sdADC were obtained, however, upon pair comparison between both spectra revealed a series of singly charged fragment ions in the sdADC spectrum that were not detected in the sdAb fragmentation pattern (**Figure 2B and 2C**) covering the 500-1400 m/z range. Upon calculation of the mass difference between each consecutive singly-charged ion, it was concluded that those ions corresponded to the fragmentation of the five last residues of the C-terminal side of the sdADC (VTVSSG, **Figure 2A**). Additionally, one ion at 776.165 *m/z* value was observed, corresponding to the AF488 molecule conjugated to the cysteamine residue. According to these signature ions, the conjugation of the surrogate cytotoxic payload molecule occurred on the thiol group of the cysteamine residue located in the C-terminal side of the protein.

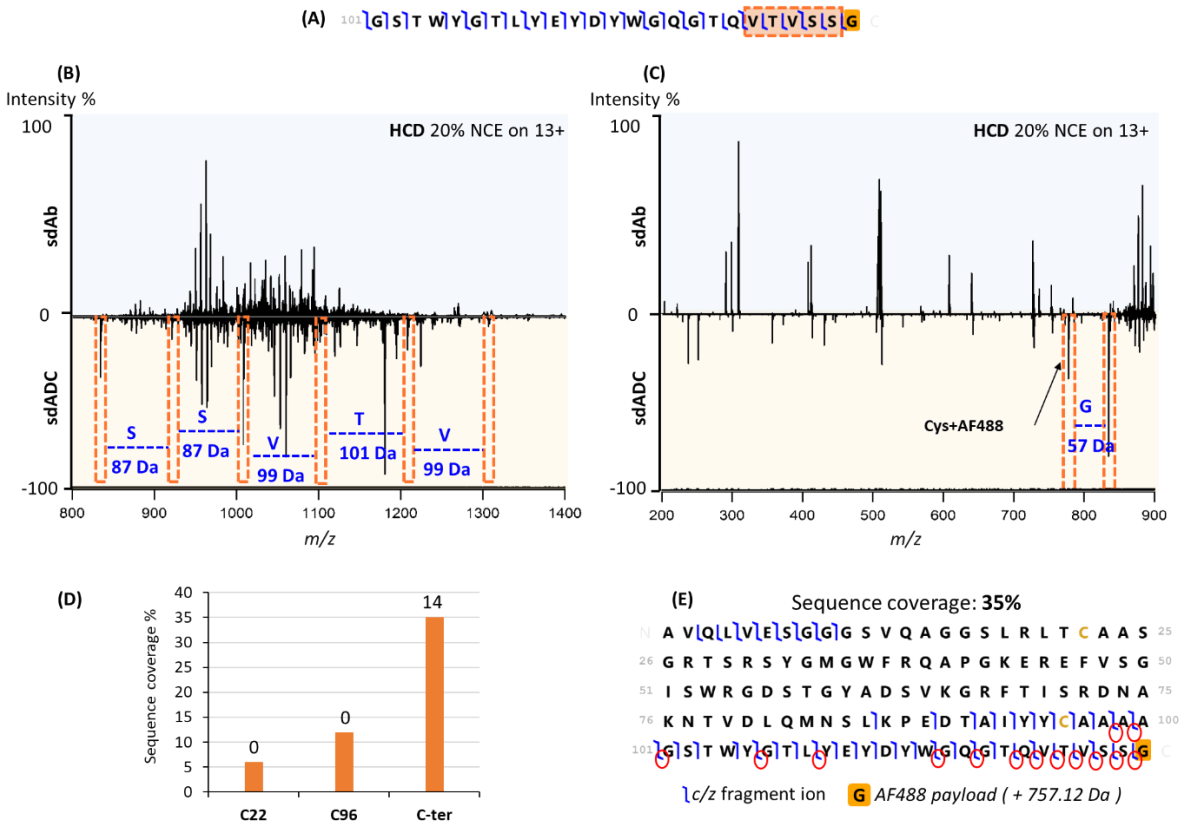

Figure 2: TD-MS experiments of sdADC. (**A**) Sequence coverage of the sdADC upon 20% NCE HCD, focused on the C-terminal region bearing the AF488 modification.(**B and C**) MS/MS spectra upon 20% NCE HCD fragmentation of sdAb (top) and sdADC (bottom) showing new fragment ions in the case of the sdADC corresponding to the AF488 modification. (**D**) Histogram representing the sequence coverage with the different positions. The numbers on the bars represent the specific fragment to the modification. (**E**) Fragmentation map of matched c/z ions with the sdADC sequence. AF488 modification is outlined in an orange frame. Specific fragments are depicted with red circles

To further strengthen this result, the variation of the sequence coverage of the sdADC as a function of the AF488 position was assessed (**Figure 2D**). Since the conjugations strategy relied on the site selective maleimide-thiol reaction, the fragment ions were matched with three different sdADC sequences containing the AF488 molecule at position cys26, cys96, and cysteamine 125. Thus, fragment ion matching with the conjugation site located at position Cys26, and Cys96 led to a poor sequence coverage of 6, and 12% respectively with no *b*-ions containing the aforementioned conjugated cysteine residues (**Figure 2C and S5**). Conversely, the sequence coverage rose to 35% when the conjugated molecule was located at the C-terminal side (cysteamine conjugation), providing 14 diagnostic *y*-fragment ions of the position of the AF488 molecule in the cysteamine thiol group (**Figure 2D and 2E**). Overall, these results are in line with the singly-charged diagnostic fragments observed upon spectra comparison between the conjugated and naked sdAb, thus leading to the unambiguous conclusion that the conjugation of the sdADC was selectively performed in the C-terminal side of the sdADC. This result was in line with data obtained through peptide mapping analysis. Upon digestion of the sdADC, only one AF488-bound peptide was found corresponding to the peptide covering the 117-125 region

of the protein (**Figure S6**). Combination of TD-MS, and peptide mapping data clearly corroborates the selectivity of the bioconjugation strategy used to modify the initial sdAb.

Benefits of ETD and UVPD for extended sdADC sequencing

Although the conjugation site is perfectly localized with the sole use of HCD, the fragmentation yield remains relatively low for a 14 kDa protein (35%). In order to provide a more extensive sequence characterization, the use of complementary activation techniques such as ETD, and UVPD were also performed. These two techniques have been shown to provide higher sequence coverage in comparison to collision-based fragmentations, covering in a more efficient manner the interior regions of protein backbones.[33-34, 36, 39, 66]

ETD, and UVPD reaction conditions were chosen from the optimal conditions of the fragmentation of the reduced sdAb. Thus, the optimal ETD reaction time was 4 ms whereas 20 ms of irradiation time was chosen in the case of UVPD activation.These experimental parameters led to 52%, and 55% of sequence coverage of the sdADC, respectively (**Figure S7-S8**), increasing significantly the sequence coverage obtained with HCD, as expected.

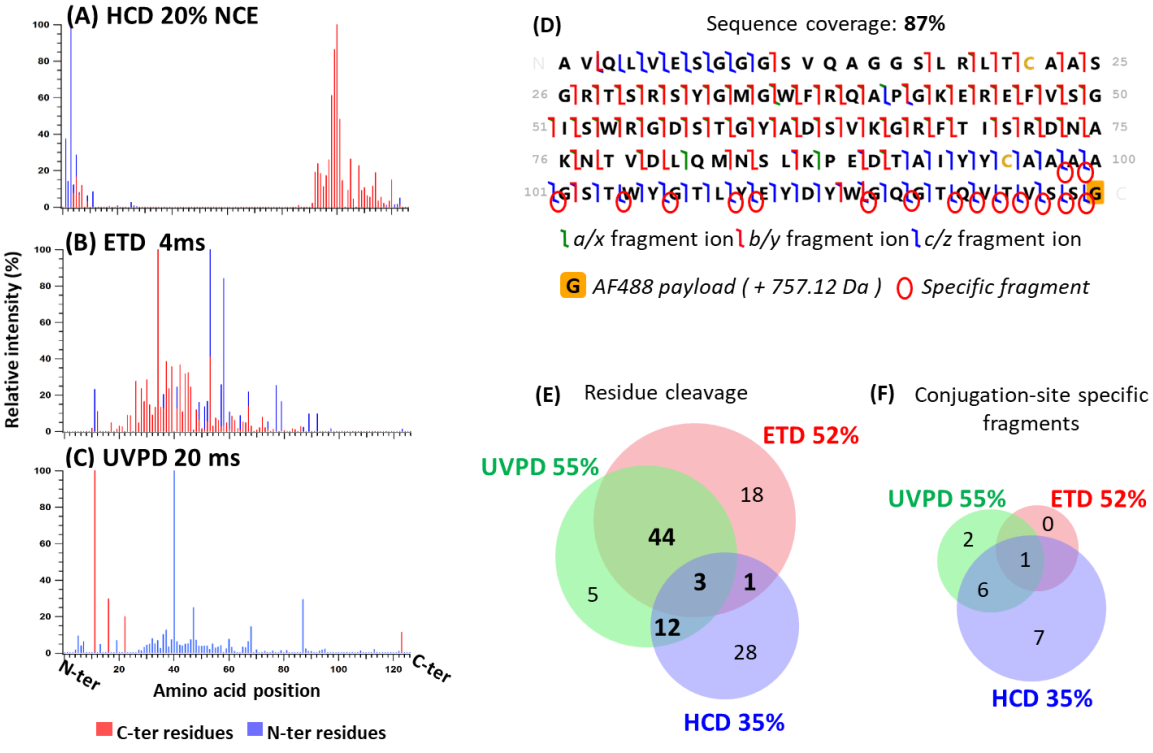

Figure 3: Location of C-terminal and N-terminal residues upon sdADC fragmentation using (**A**) 20% NCE HCD, (**B**) 4 ms ETD and (**C**) 20 ms 213 nm UVPD. (**D**) Total sequence coverage after combination of the three results. AF488 modification is outlined in a green frame and specific fragments are depicted in red circles. (**E**) Residue cleavage of the different fragmentation techniques with shared and common fragments. (**F**) Number of specific fragments to the C-ter modification upon HCD, ETD and UVPD.

According to the ion maps of ETD, and UVPD fragmentations, the mid regions of the sdADC were efficiently fragmented, especially between the 26, and 76 residues where the sequence coverage was 94%, and 82% for the ETD, and UVPD respectively (**Figure S8C-D**). This region was poorly characterized with HCD fragmentation), highlighting the great interest of combining orthogonal fragmentation techniques for an enhanced sequence coverage. Thus, ETD, and UVPD afforded complementary results in comparison with HCD, with only three fragments shared by the three fragmentation techniques (less than 2%), raising the overall sdADC sequencing to 87% (**Figure S9**). However, the latter techniques were not very informative regarding the C-terminal side, and hence the conjugation site of the protein. ETD only provided with one specific fragment of the conjugation site of the sdADC (z_{11}), and 9 fragments were observed in the case of UVPD. Interestingly, 6 consecutive signature fragment ions from val121, to gly125 identified in the UVPD spectrum were assigned to *y*-type fragment ions that were not generated during the fragmentation of the sdAb. One possible explanation that could account for this particular fragmentation behavior could be related with the presence of the AF488 molecule in the structure of the protein. The chromophore of the AF488 molecule could increase the photon absorption in the C-terminal side of the protein, favoring the CID-like fragmentation mechanism of the UVPD in the adjacent residues of the C-terminal site (QVTVSSG). Of note, despite HCD offering the lowest sequence coverage, it remained the most suitable method to decipher the conjugation site with 14 fragment ions characteristic of the AF488 conjugation at the C-terminal side.

TD-MS fragmentation of intact sdADC for direct evidence of intra-molecular disulfide bond preservation

TD-MS strategies have been also applied to proteins with inter,[48, 51, 67-69] and intra-disulfide links.[48, 51, 64-65, 68-71] In some cases, different fragmentation techniques were used to disrupt the disulfide bonds of the proteins with the main purpose of increasing the overall fragmentation yield, and hence provide a better primary structure characterization. Even though collisional activation techniques can potentially fragment disulfide bonds,[70-71] electron-driven fragmentation of photo-dissociation techniques have been shown a more marked propensity to disrupt cysteine-linked proteins either by promoting a S-S homolytic fragmentation mechanism (accompanied or not by a hydrogen transfer)[67, 72] or breaking the C-S bonds.[48, 64, 73] These fragmentation mechanisms give rise to diagnostic fragment ions that can be capitalized upon, along with the identification of backbone fragments containing oxidized cysteine residues (H loss modification), not only to increase the overall sequence coverage but also, to decipher the disulfide patterns of proteins with intra- and inter-molecular disulfide linkages. Thereby, the different activation methods included in the current study were used to generate specific fragments of the disulfide bond contained within the structure of the sdADC between

the two cysteine residues to provide further evidence about the disulfide linkage integrity upon the conjugation process.

The mass spectrum of the non-reduced sdADC clearly shows a dramatic reduction of the overall charge state (**Figure 4A**) compared to the mass spectrum of the reduced sample. The charge state distribution of the reduced sdADC was centered at the 13+ charge state while the most intense species of the non-reduced sample is the 6+ charge state. This is consistent with the fact that almost 60% of the sdADC sequence is flanked by the disulfide bond, leading to a more folded structure which precludes the protonation of the protein, and thus reduces the overall charge state. This characteristic will presumably impair the fragmentation efficiency of the different fragmentation techniques due to both the selection of lower charge state precursor ions, and the hindrance for the internal energy redistribution throughout the whole sdADC sequence. The 6+ charge state precursor ion was isolated and subjected to the fragmentation with the three activation techniques, *i.e.* HCD, ETD, and UVPD. Overall, the sequence coverage afforded by the three techniques drastically decreased compared to the reduced sdADC. HCD, and ETD methods provided fragments on the protein regions that were not enclosed by the S-S bond, covering the N-, and C-termini of the sdADC with a series of *y*-(HCD), and *c*-ion fragments (ETD) (**Figure 4B and S10-11**). In both cases, *y*-, and *c*-ions pinpointed the presence of both cysteine residues in their oxidized form (*i.e.* involved in the intra-molecular bond). Additionally, the fragment ions resulting from the HCD activation contained the C-terminal side of the protein bearing the AF488 molecule, thus simultaneously corroborating the presence of the disulfide bond of the protein along with the precise conjugation site. In spite of the marked selectivity of ETD fragmentation to excise disulfide bonds, hallmarks of disulfide bond cleavage could not be found upon ETD activation. UVPD showed enhanced fragmentation yield, providing 22% of intact sdADC sequence coverage. In this case, fragment ions in the region enclosed by the disulfide bond were produced, corresponding to a homolytic S-S cleavage without, in principle, hydrogen transfer (**Figure 4C and S12**).

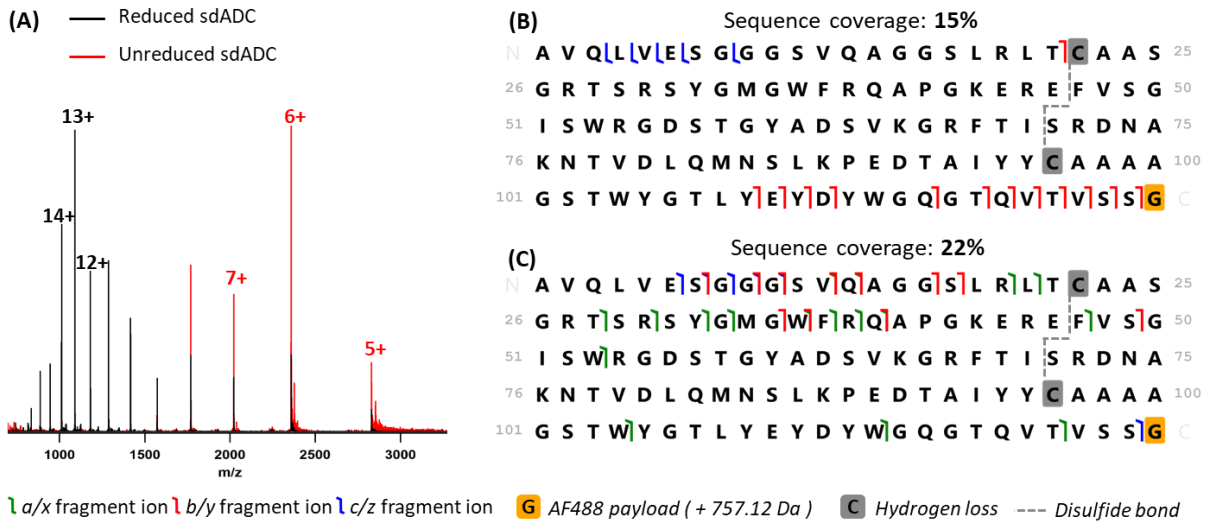

Figure 4: TD-MS experiments of unreduced sdADC performed on the 6+ charge state precursor ion. **(A)** Comparison of MS spectra from rpLC-MS analysis of reduced sdADC (black line) *versus* unreduced sdADC (red line) showing the different charge envelopes. **(B)** Fragmentation map upon 10% NCE HCD and 6 ms ETD and **(C)** upon 30 ms 213 nm UVPD. AF488 modification is outlined in orange frame and hydrogen loss modifications are in grey frames. The disulfide bond is depicted in grey dashed line.

In order to dig deeper on the identification of produced fragments from the intact sdADC, fragment ion search space was extended to internal fragments. Therefore, ClipsMS[74] was used to identify fragment ions resulting from multiple protein backbone fragmentation events. The inclusion of internal fragments in the ion searching has been shown beneficial in terms of overall sequence coverage of cysteine-rich proteins, providing an extensive primary sequence characterization.[41, 65, 70-71] In the particular case of the sdADC, these ions were exclusively used to identify fragments ions related with the presence of the disulfide bond, *i.e.* either containing both cysteine residues oxidized, or fragments resulting from the dissociation of the disulfide bond. After manual validation, no internal fragments could be confirmed for HCD, and ETD methods while 10 internal fragments containing the intact disulfide bridge could be matched upon UVPD fragmentation (**Figure 5 and S13**) providing more specific and straight evidences about the presence of the S-S intra-link. Unfortunately, the triplet fragment ion signature (C-S fragmentation) and additional homolytic S-S dissociation were not confirmed.

One of the reasons that may lead to the absence of disulfide bond cleavage fragment ions identification stems from the reduced acquisition time of the MS2 spectra due to the coupling of the LC dimension in the forefront of the mass spectrometer. Most of the studies that envisaged the fragmentation of intact protein with multiple disulfide bonds are conducted in direct infusion, recording the fragmentation spectra during several hundreds of transients.[48, 63-65, 67, 70-72] This is a key parameter that facilitates the identification of low abundant ions by increasing the S/N ratio alongside the acquisition time. This is even more important for diagnostic fragments characteristics of the disulfide bond

fragmentation, which relative intensity has been estimated to be less than 5% of the total fragment ion intensity.[63] According to this result, it is highly likely that the reduced acquisition time of the LC-TD-MS spectrum of the sdADC (FWHM 0.11 min) precludes the detection of these low-abundant fragment ions. However, the results recorded with the three fragmentation techniques clearly demonstrate the connectivity of the S-S bond from the Cys22 to the Cys96 residues after confirming the presence of terminal and internal fragments containing both oxidized cysteine residues. The contribution of both types of ions clearly led to the confirmation of disulfide linkage of both cysteine residues, and thus providing a more comprehensive characterization of the nanobody structure.

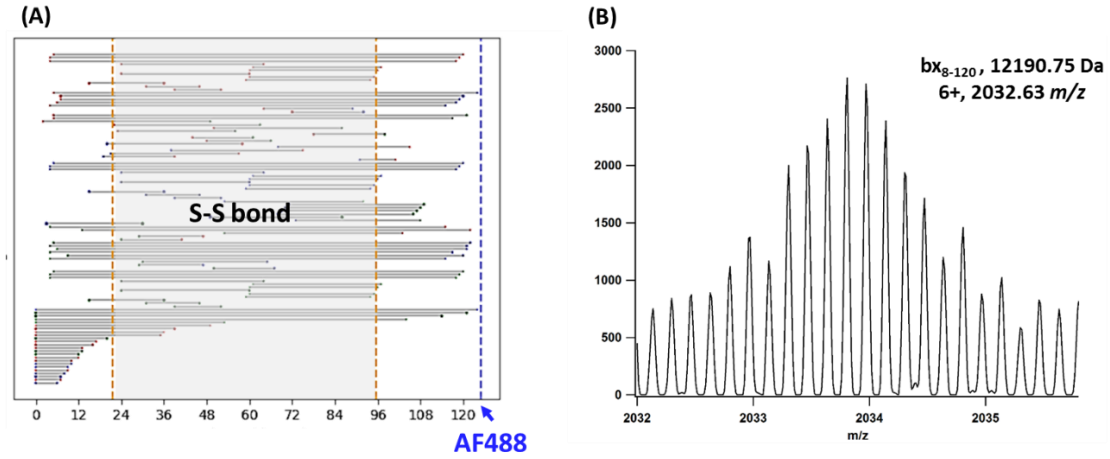

Figure 5: Added value of internal fragments consideration for the identification of the disulfide bond on the unreduced form of the sdADC. **(A)** Fragments location map upon 30 ms UVPD. Orange dashed lines represent the position of the cysteines involved in the S-S bond and blue dashed line represent the position of the AF488 modification. **(B)** Isotopic profile of an internal fragment *(bx_{8-120})* bearing both cysteines involved in the S-S bond.

4. Conclusions

The current study reports for the first time on the characterization of a sdADC conjugated with a surrogate cytotoxic payload molecule using an optimized LC-TD-MS workflow based on three different activation techniques, *i.e.* HCD, ETD, and UVPD. The results clearly highlight the benefits and limitations of all the three techniques in terms of sequence coverage, conjugation site, and determination/fragmentation of intramolecular disulfide bonds in order to afford the most comprehensive characterization of the sdADC primary structure.

Upon unveiling the number of conjugated molecules attached to the sdAb sequence, the conjugated protein was interrogated with the three different activation methods. As expected by previous analyses, ETD, and UVPD provided extensive sequence characterization, especially in the mid-region of the sdADC. However, HCD fragmentation was more informative regarding the number of fragment ions that were diagnostic to the specific conjugation site. This result seems to disagree with previous

studies where electron- and photo-dissociation techniques outperformed the results of collisional activation techniques.[34-36] Two main reasons can account for this observation. The first one is that the conjugation site of the sdADC is located in the C-terminal extremity, a region which is normally well sequenced by collisional activation techniques. The second one is that the structure of the cargo molecule used in this study does not contain an ester bond that is commonly used to covalently attach the cytotoxic molecule to the linker of more classical ADC payloads. As a consequence, the AF488 moiety exhibits more resistance to undergo fragmentation, and thus remaining intact upon collisions with the background gas.

The LC-TD-MS workflow was also applied to the non-reduced sdADC sample to determine the presence of the intramolecular S-S bond after conjugation of the AF488 molecule. The fragmentation efficiency of the three techniques drastically decreased since the disulfide bond stabilizes the secondary structure of the protein leading to a more compact, and less charged entity. The overall sequence coverage upon combination of the three techniques led to a final 33%. Only a limited number of fragment ions characteristics of the disulfide bond cleavage were identified upon UVPD fragmentation. This is in good agreement with previous studies showing that UVPD is less sensitive to the net charge state of the precursor ion,[75-76] and affords a marked propensity to fragment disulfide bonds.[67, 77] The vast majority of fragment ions stemmed from the fragmentation of the regions near the N-, and C-termini that were not encompassed by the intra-molecular bond. Nevertheless, these ions (either terminal or internal ions) corroborated the presence of the disulfide bridge along with the localization of the AF488 molecule in the C-terminal side.

Altogether, these results put in evidence that despite the relatively low molecular weight, and the limited structural heterogeneity, the fragmentation and comprehensive characterization of sdAb, and sdADCs at the intact level is still challenge, especially when TD-MS experimental workflows are conducted in the chromatography time scale. However, the use of complementary activation techniques, and tailored fragment ion searches can boost the performances of these workflows in terms of sequence coverage and signature fragment ions, spurring their application to the characterization of a large array of proteins.

5. References

1. Crescioli, S.,Kaplon, H.,Chenoweth, A.,Wang, L.,Visweswaraiah, J.,Reichert, J. M.: Antibodies to watch in 2024. MAbs 16 (1), 2297450 (2024).
2. Jin, B. K.,Odongo, S.,Radwanska, M.,Magez, S.: Nanobodies: A Review of Generation, Diagnostics and Therapeutics. International journal of molecular sciences 24 (6), (2023).
3. Yong Joon Kim, J.,Sang, Z.,Xiang, Y.,Shen, Z.,Shi, Y.: Nanobodies: Robust miniprotein binders in biomedicine. Advanced drug delivery reviews 195 114726 (2023).
4. Hamers-Casterman, C.,Atarhouch, T.,Muyldermans, S.,Robinson, G.,Hammers, C.,Songa, E. B.,Bendahman, N.,Hammers, R.: Naturally occurring antibodies devoid of light chains. Nature 363 (6428), 446-448 (1993).

5. Greenberg, A. S.,Avila, D.,Hughes, M.,Hughes, A.,McKinney, E. C.,Flajnik, M. F.: A new antigen receptor gene family that undergoes rearrangement and extensive somatic diversification in sharks. Nature 374 (6518), 168-173 (1995).
6. Kijanka, M.,Dorresteijn, B.,Oliveira, S.,van Bergen en Henegouwen, P. M.: Nanobody-based cancer therapy of solid tumors. Nanomedicine (London, England) 10 (1), 161-74 (2015).
7. Wang, L.,Zhang, G.,Qin, L.,Ye, H.,Wang, Y.,Long, B.,Jiao, Z.: Anti-EGFR Binding Nanobody Delivery System to Improve the Diagnosis and Treatment of Solid Tumours. Recent patents on anti-cancer drug discovery 15 (3), 200-211 (2020).
8. Bélanger, K.,Iqbal, U.,Tanha, J.,MacKenzie, R.,Moreno, M.,Stanimirovic, D.: Single-Domain Antibodies as Therapeutic and Imaging Agents for the Treatment of CNS Diseases. Antibodies (Basel, Switzerland) 8 (2), (2019).
9. Pothin, E.,Lesuisse, D.,Lafaye, P.: Brain Delivery of Single-Domain Antibodies: A Focus on VHH and VNAR. Pharmaceutics 12 (10), (2020).
10. Henry, K. A.,MacKenzie, C. R.: Antigen recognition by single-domain antibodies: structural latitudes and constraints. MAbs 10 (6), 815-826 (2018).
11. De Genst, E.,Silence, K.,Decanniere, K.,Conrath, K.,Loris, R.,Kinne, J.,Muyldermans, S.,Wyns, L.: Molecular basis for the preferential cleft recognition by dromedary heavy-chain antibodies. Proc Natl Acad Sci U S A 103 (12), 4586-91 (2006).
12. Ackaert, C.,Smiejkowska, N.,Xavier, C.,Sterckx, Y. G. J.,Denies, S.,Stijlemans, B.,Elkrim, Y.,Devoogdt, N.,Caveliers, V.,Lahoutte, T.,Muyldermans, S.,Breckpot, K.,Keyaerts, M.: Immunogenicity Risk Profile of Nanobodies. Frontiers in immunology 12 632687 (2021).
13. Rossotti, M. A.,Bélanger, K.,Henry, K. A.,Tanha, J.: Immunogenicity and humanization of single-domain antibodies. The FEBS journal 289 (14), 4304-4327 (2022).
14. Wang, Y.,Fan, Z.,Shao, L.,Kong, X.,Hou, X.,Tian, D.,Sun, Y.,Xiao, Y.,Yu, L.: Nanobody-derived nanobiotechnology tool kits for diverse biomedical and biotechnology applications. International journal of nanomedicine 11 3287-303 (2016).
15. Dumoulin, M.,Conrath, K.,Van Meirhaeghe, A.,Meersman, F.,Heremans, K.,Frenken, L. G.,Muyldermans, S.,Wyns, L.,Matagne, A.: Single-domain antibody fragments with high conformational stability. Protein Sci. 11 (3), 500-15 (2002).
16. Ruano-Gallego, D.,Fraile, S.,Gutierrez, C.,Fernández, L. Á.: Screening and purification of nanobodies from E. coli culture supernatants using the hemolysin secretion system. Microbial Cell Factories 18 (1), 47 (2019).
17. Gorlani, A.,de Haard, H.,Verrips, T.: Expression of VHHs in Saccharomyces cerevisiae. Methods in molecular biology (Clifton, N.J.) 911 277-86 (2012).
18. Mei, Y.,Chen, Y.,Sivaccumar, J. P.,An, Z.,Xia, N.,Luo, W.: Research progress and applications of nanobody in human infectious diseases. Frontiers in pharmacology 13 963978 (2022).
19. Liu, M.,Li, L.,Jin, D.,Liu, Y.: Nanobody-A versatile tool for cancer diagnosis and therapeutics. Wiley interdisciplinary reviews. Nanomedicine and nanobiotechnology 13 (4), e1697 (2021).
20. Gao, Y.,Zhu, J.,Lu, H.: Single domain antibody-based vectors in the delivery of biologics across the blood-brain barrier: a review. Drug delivery and translational research 11 (5), 1818-1828 (2021).
21. Pronk, S. D.,Schooten, E.,Heinen, J.,Helfrich, E.,Oliveira, S.,van Bergen En Henegouwen, P. M. P.: Single Domain Antibodies as Carriers for Intracellular Drug Delivery: A Proof of Principle Study. Biomolecules 11 (7), (2021).
22. Barakat, S.,Berksöz, M.,Zahedimaram, P.,Piepoli, S.,Erman, B.: Nanobodies as molecular imaging probes. Free radical biology & medicine 182 260-275 (2022).
23. Brown, K. A.,Tucholski, T.,Alpert, A. J.,Eken, C.,Wesemann, L.,Kyrvasilis, A.,Jin, S.,Ge, Y.: Top-Down Proteomics of Endogenous Membrane Proteins Enabled by Cloud Point Enrichment and Multidimensional Liquid Chromatography-Mass Spectrometry. Anal. Chem. 92 (24), 15726-15735 (2020).
24. Juliano, B. R.,Keating, J. W.,Ruotolo, B. T.: Infrared Photoactivation Enables Improved Native Top-Down Mass Spectrometry of Transmembrane Proteins. Anal. Chem. 95 (35), 13361-13367 (2023).
25. Lutomski, C. A.,El-Baba, T. J.,Hinkle, J. D.,Liko, I.,Bennett, J. L.,Kalmankar, N. V.,Dolan, A.,Kirschbaum, C.,Greis, K.,Urner, L. H.,Kapoor, P.,Yen, H. Y.,Pagel, K.,Mullen, C.,Syka, J. E. P.,Robinson, C. V.: Infrared Multiphoton Dissociation Enables Top-Down Characterization of Membrane Protein Complexes and G Protein-Coupled Receptors. Angew. Chem. Int. Ed. Engl. 62 (36), e202305694 (2023).
26. Gault, J.,Liko, I.,Landreh, M.,Shutin, D.,Bolla, J. R.,Jefferies, D.,Agasid, M.,Yen, H. Y.,Ladds, M.,Lane, D. P.,Khalid, S.,Mullen, C.,Remes, P. M.,Huguet, R.,McAlister, G.,Goodwin, M.,Viner, R.,Syka, J. E. P.,Robinson, C. V.: Combining native and 'omics' mass spectrometry to identify endogenous ligands bound to membrane proteins. Nat Methods 17 (5), 505-508 (2020).
27. Walker, J. N.,Lam, R.,Brodbelt, J. S.: Enhanced Characterization of Histones Using 193 nm Ultraviolet Photodissociation and Proton Transfer Charge Reduction. Anal. Chem. 95 (14), 5985-5993 (2023).
28. Berthias, F.,Thurman, H. A.,Wijegunawardena, G.,Wu, H.,Shvartsburg, A. A.,Jensen, O. N.: Top-Down Ion Mobility Separations of Isomeric Proteoforms. Anal. Chem. 95 (2), 784-791 (2023).
29. Jeanne Dit Fouque, K.,Miller, S. A.,Pham, K.,Bhanu, N. V.,Cintron-Diaz, Y. L.,Leyva, D.,Kaplan, D.,Voinov, V. G.,Ridgeway, M. E.,Park, M. A.,Garcia, B. A.,Fernandez-Lima, F.: Top-"Double-Down" Mass Spectrometry of Histone H4 Proteoforms: Tandem Ultraviolet-Photon and Mobility/Mass-Selected Electron Capture Dissociations. Anal. Chem. 94 (44), 15377-15385 (2022).
30. Peters-Clarke, T. M.,Quan, Q.,Brademan, D. R.,Hebert, A. S.,Westphall, M. S.,Coon, J. J.: Ribonucleic Acid Sequence Characterization by Negative Electron Transfer Dissociation Mass Spectrometry. Anal. Chem. 92 (6), 4436-4444 (2020).

31. Santos, I. C.,Lanzillotti, M.,Shilov, I.,Basanta-Sanchez, M.,Roushan, A.,Lawler, R.,Tang, W.,Bern, M.,Brodbelt, J. S.: Ultraviolet Photodissociation and Activated Electron Photodetachment Mass Spectrometry for Top-Down Sequencing of Modified Oligoribonucleotides. J. Am. Soc. Mass. Spectrom. 33 (3), 510-520 (2022).
32. Crittenden, C. M.,Lanzillotti, M. B.,Chen, B.: Top-Down Mass Spectrometry of Synthetic Single Guide Ribonucleic Acids Enabled by Facile Sample Clean-Up. Anal. Chem. 95 (6), 3180-3186 (2023).
33. Dhenin, J.,Dupré, M.,Druart, K.,Krick, A.,Mauriac, C.,Chamot-Rooke, J.: A multiparameter optimization in middle-down analysis of monoclonal antibodies by LC-MS/MS. J. Mass Spectrom. 58 (3), e4909 (2023).
34. Beaumal, C.,Deslignière, E.,Diemer, H.,Carapito, C.,Cianférani, S.,Hernandez-Alba, O.: Improved characterization of trastuzumab deruxtecan with PTCR and internal fragments implemented in middle-down MS workflows. Anal Bioanal Chem (2023).
35. Watts, E.,Williams, J. D.,Miesbauer, L. J.,Bruncko, M.,Brodbelt, J. S.: Comprehensive Middle-Down Mass Spectrometry Characterization of an Antibody-Drug Conjugate by Combined Ion Activation Methods. Anal. Chem. 92 (14), 9790-9798 (2020).
36. Hernandez-Alba, O.,Houel, S.,Hessmann, S.,Erb, S.,Rabuka, D.,Huguet, R.,Josephs, J.,Beck, A.,Drake, P. M.,Cianférani, S.: A Case Study to Identify the Drug Conjugation Site of a Site-Specific Antibody-Drug-Conjugate Using Middle-Down Mass Spectrometry. J. Am. Soc. Mass. Spectrom. 30 (11), 2419-2429 (2019).
37. Chen, B.,Lin, Z.,Zhu, Y.,Jin, Y.,Larson, E.,Xu, Q.,Fu, C.,Zhang, Z.,Zhang, Q.,Pritts, W. A.,Ge, Y.: Middle-Down Multi-Attribute Analysis of Antibody-Drug Conjugates with Electron Transfer Dissociation. Anal. Chem. 91 (18), 11661-11669 (2019).
38. Srzentic, K.,Nagornov, K. O.,Fornelli, L.,Lobas, A. A.,Ayoub, D.,Kozhinov, A. N.,Gasilova, N.,Menin, L.,Beck, A.,Gorshkov, M. V.,Aizikov, K.,Tsybin, Y. O.: Multiplexed Middle-Down Mass Spectrometry as a Method for Revealing Light and Heavy Chain Connectivity in a Monoclonal Antibody. Anal. Chem. 90 (21), 12527-12535 (2018).
39. Cotham, V. C.,Brodbelt, J. S.: Characterization of Therapeutic Monoclonal Antibodies at the Subunit-Level using Middle-Down 193 nm Ultraviolet Photodissociation. Anal. Chem. 88 (7), 4004-4013 (2016).
40. Fornelli, L.,Ayoub, D.,Aizikov, K.,Beck, A.,Tsybin, Y. O.: Middle-Down Analysis of Monoclonal Antibodies with Electron Transfer Dissociation Orbitrap Fourier Transform Mass Spectrometry. Anal. Chem. 86 (6), 3005-3012 (2014).
41. Wei, B.,Lantz, C.,Ogorzalek Loo, R. R.,Campuzano, I. D. G.,Loo, J. A.: Internal Fragments Enhance Middle-Down Mass Spectrometry Structural Characterization of Monoclonal Antibodies and Antibody-Drug Conjugates. Anal. Chem. (2024).
42. Melani, R. D.,Srzentić, K.,Gerbasi, V. R.,McGee, J. P.,Huguet, R.,Fornelli, L.,Kelleher, N. L.: Direct measurement of light and heavy antibody chains using ion mobility and middle-down mass spectrometry. MAbs 11 (8), 1351-1357 (2019).
43. Fornelli, L.,Damoc, E.,Thomas, P. M.,Kelleher, N. L.,Aizikov, K.,Denisov, E.,Makarov, A.,Tsybin, Y. O.: Analysis of Intact Monoclonal Antibody IgG1 by Electron Transfer Dissociation Orbitrap FTMS. Molecular & Cellular Proteomics 11 (12), 1758-1767 (2012).
44. Tsybin, Y. O.,Fornelli, L.,Stoermer, C.,Luebeck, M.,Parra, J.,Nallet, S.,Wurm, F. M.,Hartmer, R.: Structural Analysis of Intact Monoclonal Antibodies by Electron Transfer Dissociation Mass Spectrometry. Anal. Chem. 83 (23), 8919-8927 (2011).
45. Fornelli, L.,Ayoub, D.,Aizikov, K.,Liu, X.,Damoc, E.,Pevzner, P. A.,Makarov, A.,Beck, A.,Tsybin, Y. O.: Top-down analysis of immunoglobulin G isotypes 1 and 2 with electron transfer dissociation on a high-field Orbitrap mass spectrometer. Journal of proteomics 159 67-76 (2017).
46. Mao, Y.,Valeja, S. G.,Rouse, J. C.,Hendrickson, C. L.,Marshall, A. G.: Top-Down Structural Analysis of an Intact Monoclonal Antibody by Electron Capture Dissociation-Fourier Transform Ion Cyclotron Resonance-Mass Spectrometry. Anal. Chem. 85 (9), 4239-4246 (2013).
47. Lodge, J. M.,Schauer, K. L.,Brademan, D. R.,Riley, N. M.,Shishkova, E.,Westphall, M. S.,Coon, J. J.: Top-Down Characterization of an Intact Monoclonal Antibody Using Activated Ion Electron Transfer Dissociation. Anal. Chem. 92 (15), 10246-10251 (2020).
48. Shaw, J. B.,Liu, W.,Vasil Ev, Y. V.,Bracken, C. C.,Malhan, N.,Guthals, A.,Beckman, J. S.,Voinov, V. G.: Direct Determination of Antibody Chain Pairing by Top-down and Middle-down Mass Spectrometry Using Electron Capture Dissociation and Ultraviolet Photodissociation. Anal. Chem. 92 (1), 766-773 (2020).
49. Srzentić, K.,Fornelli, L.,Tsybin, Y. O.,Loo, J. A.,Seckler, H.,Agar, J. N.,Anderson, L. C.,Bai, D. L.,Beck, A.,Brodbelt, J. S.,van der Burgt, Y. E. M.,Chamot-Rooke, J.,Chatterjee, S.,Chen, Y.,Clarke, D. J.,Danis, P. O.,Diedrich, J. K.,D'Ippolito, R. A.,Dupré, M.,Gasilova, N.,Ge, Y.,Goo, Y. A.,Goodlett, D. R.,Greer, S.,Haselmann, K. F.,He, L.,Hendrickson, C. L.,Hinkle, J. D.,Holt, M. V.,Hughes, S.,Hunt, D. F.,Kelleher, N. L.,Kozhinov, A. N.,Lin, Z.,Malosse, C.,Marshall, A. G.,Menin, L.,Millikin, R. J.,Nagornov, K. O.,Nicolardi, S.,Paša-Tolić, L.,Pengelley, S.,Quebbemann, N. R.,Resemann, A.,Sandoval, W.,Sarin, R.,Schmitt, N. D.,Shabanowitz, J.,Shaw, J. B.,Shortreed, M. R.,Smith, L. M.,Sobott, F.,Suckau, D.,Toby, T.,Weisbrod, C. R.,Wildburger, N. C.,Yates, J. R., 3rd,Yoon, S. H.,Young, N. L.,Zhou, M.: Interlaboratory Study for Characterizing Monoclonal Antibodies by Top-Down and Middle-Down Mass Spectrometry. J. Am. Soc. Mass. Spectrom. 31 (9), 1783-1802 (2020).
50. Fornelli, L.,Srzentić, K.,Huguet, R.,Mullen, C.,Sharma, S.,Zabrouskov, V.,Fellers, R. T.,Durbin, K. R.,Compton, P. D.,Kelleher, N. L.: Accurate Sequence Analysis of a Monoclonal Antibody by Top-Down and Middle-Down Orbitrap Mass Spectrometry Applying Multiple Ion Activation Techniques. Anal. Chem. 90 (14), 8421-8429 (2018).

51. Wei, B.,Lantz, C.,Liu, W.,Viner, R.,Ogorzalek Loo, R. R.,Campuzano, I. D. G.,Loo, J. A.: Added Value of Internal Fragments for Top-Down Mass Spectrometry of Intact Monoclonal Antibodies and Antibody–Drug Conjugates. Anal. Chem. (2023).
52. Larson, E. J.,Roberts, D. S.,Melby, J. A.,Buck, K. M.,Zhu, Y.,Zhou, S.,Han, L.,Zhang, Q.,Ge, Y.: High-Throughput Multi-attribute Analysis of Antibody-Drug Conjugates Enabled by Trapped Ion Mobility Spectrometry and Top-Down Mass Spectrometry. Anal. Chem. 93 (29), 10013-10021 (2021).
53. Resemann, A.,Wunderlich, D.,Rothbauer, U.,Warscheid, B.,Leonhardt, H.,Fuchser, J.,Kuhlmann, K.,Suckau, D.: Top-down de Novo protein sequencing of a 13.6 kDa camelid single heavy chain antibody by matrix-assisted laser desorption ionization-time-of-flight/time-of-flight mass spectrometry. Anal. Chem. 82 (8), 3283-92 (2010).
54. Macias, L. A.,Wang, X.,Davies, B. W.,Brodbelt, J. S.: Mapping paratopes of nanobodies using native mass spectrometry and ultraviolet photodissociation. Chem Sci 13 (22), 6610-6618 (2022).
55. Rogers, H. T.,Roberts, D. S.,Larson, E. J.,Melby, J. A.,Rossler, K. J.,Carr, A. V.,Brown, K. A.,Ge, Y.: Comprehensive Characterization of Endogenous Phospholamban Proteoforms Enabled by Photocleavable Surfactant and Top-down Proteomics. Anal. Chem. 95 (35), 13091-13100 (2023).
56. Dunham, S. D.,Wei, B.,Lantz, C.,Loo, J. A.,Brodbelt, J. S.: Impact of Internal Fragments on Top-Down Analysis of Intact Proteins by 193 nm UVPD. J Proteome Res 22 (1), 170-181 (2023).
57. Brodbelt, J. S.: Deciphering combinatorial post-translational modifications by top-down mass spectrometry. Curr. Opin. Chem. Biol. 70 102180 (2022).
58. Greer, S. M.,Brodbelt, J. S.: Top-Down Characterization of Heavily Modified Histones Using 193 nm Ultraviolet Photodissociation Mass Spectrometry. J Proteome Res 17 (3), 1138-1145 (2018).
59. Miller, S. A.,Jeanne Dit Fouque, K.,Hard, E. R.,Balana, A. T.,Kaplan, D.,Voinov, V. G.,Ridgeway, M. E.,Park, M. A.,Anderson, G. A.,Pratt, M. R.,Fernandez-Lima, F.: Top/Middle-Down Characterization of α-Synuclein Glycoforms. Anal. Chem. 95 (49), 18039-18045 (2023).
60. Fornelli, L.,Parra, J.,Hartmer, R.,Stoermer, C.,Lubeck, M.,Tsybin, Y. O.: Top-down analysis of 30-80 kDa proteins by electron transfer dissociation time-of-flight mass spectrometry. Analytical and Bioanalytical Chemistry 405 (26), 8505-8514 (2013).
61. Kline, J. T.,Mullen, C.,Durbin, K. R.,Oates, R. N.,Huguet, R.,Syka, J. E. P.,Fornelli, L.: Sequential Ion-Ion Reactions for Enhanced Gas-Phase Sequencing of Large Intact Proteins in a Tribrid Orbitrap Mass Spectrometer. J. Am. Soc. Mass. Spectrom. 32 (9), 2334-2345 (2021).
62. Fornelli, L.,Srzentić, K.,Huguet, R.,Mullen, C.,Sharma, S.,Zabrouskov, V.,Fellers, R. T.,Durbin, K. R.,Compton, P. D.,Kelleher, N. L.: Accurate Sequence Analysis of a Monoclonal Antibody by Top-Down and Middle-Down Orbitrap Mass Spectrometry Applying Multiple Ion Activation Techniques. Anal. Chem. 90 (14), 8421-8429 (2018).
63. Zhang, J.,Ogorzalek Loo, R. R.,Loo, J. A.: Increasing Fragmentation of Disulfide-Bonded Proteins for Top-Down Mass Spectrometry by Supercharging. Int. J. Mass spectrom. 377 546-556 (2015).
64. Rush, M. J. P.,Riley, N. M.,Westphall, M. S.,Coon, J. J.: Top-Down Characterization of Proteins with Intact Disulfide Bonds Using Activated-Ion Electron Transfer Dissociation. Anal. Chem. 90 (15), 8946-8953 (2018).
65. Wei, B.,Zenaidee, M. A.,Lantz, C.,Williams, B. J.,Totten, S.,Ogorzalek Loo, R. R.,Loo, J. A.: Top-down mass spectrometry and assigning internal fragments for determining disulfide bond positions in proteins. Analyst 148 (1), 26-37 (2022).
66. Juetten, K. J.,Brodbelt, J. S.: Top-Down Analysis of Supercharged Proteins Using Collision-, Electron-, and Photon-Based Activation Methods. J. Am. Soc. Mass. Spectrom. 34 (7), 1467-1476 (2023).
67. Macias, L. A.,Brodbelt, J. S.: Investigation of Product Ions Generated by 193 nm Ultraviolet Photodissociation of Peptides and Proteins Containing Disulfide Bonds. J. Am. Soc. Mass. Spectrom. 33 (7), 1315-1324 (2022).
68. Gammelgaard, S. K.,Petersen, S. B.,Haselmann, K. F.,Nielsen, P. K.: Characterization of Insulin Dimers by Top-Down Mass Spectrometry. J. Am. Soc. Mass. Spectrom. 32 (8), 1910-1918 (2021).
69. Quick, M. M.,Crittenden, C. M.,Rosenberg, J. A.,Brodbelt, J. S.: Characterization of Disulfide Linkages in Proteins by 193 nm Ultraviolet Photodissociation (UVPD) Mass Spectrometry. Anal. Chem. 90 (14), 8523-8530 (2018).
70. Chen, J.,Shiyanov, P.,Zhang, L.,Schlager, J. J.,Green-Church, K. B.: Top-down characterization of a native highly intralinked protein: concurrent cleavages of disulfide and protein backbone bonds. Anal. Chem. 82 (14), 6079-89 (2010).
71. Chen, J.,Shiyanov, P.,Schlager, J. J.,Green, K. B.: A pseudo MS3 approach for identification of disulfide-bonded proteins: uncommon product ions and database search. J. Am. Soc. Mass. Spectrom. 23 (2), 225-43 (2012).
72. Zhao, X.,Shen, Y.,Tong, W.,Wang, G.,Chen, D. D. Y.: Deducing disulfide patterns of cysteine-rich proteins using signature fragments produced by top-down mass spectrometry. Analyst 143 (4), 817-823 (2018).
73. Srzentić, K.,Nagornov, K. O.,Fornelli, L.,Lobas, A. A.,Ayoub, D.,Kozhinov, A. N.,Gasilova, N.,Menin, L.,Beck, A.,Gorshkov, M. V.,Aizikov, K.,Tsybin, Y. O.: Multiplexed Middle-Down Mass Spectrometry as a Method for Revealing Light and Heavy Chain Connectivity in a Monoclonal Antibody. Anal. Chem. 90 (21), 12527-12535 (2018).
74. Lantz, C.,Zenaidee, M. A.,Wei, B.,Hemminger, Z.,Ogorzalek Loo, R. R.,Loo, J. A.: ClipsMS: An Algorithm for Analyzing Internal Fragments Resulting from Top-Down Mass Spectrometry. J Proteome Res 20 (4), 1928-1935 (2021).
75. Bashyal, A.,Sanders, J. D.,Holden, D. D.,Brodbelt, J. S.: Top-Down Analysis of Proteins in Low Charge States. J. Am. Soc. Mass. Spectrom. 30 (4), 704-717 (2019).

76. Brodbelt, J. S.,Morrison, L. J.,Santos, I.: Ultraviolet Photodissociation Mass Spectrometry for Analysis of Biological Molecules. Chem. Rev. 120 (7), 3328-3380 (2020).
77. Talbert, L. E.,Julian, R. R.: Directed-Backbone Dissociation Following Bond-Specific Carbon-Sulfur UVPD at 213 nm. J. Am. Soc. Mass. Spectrom. 29 (9), 1760-1767 (2018).